Demonstration of Radiation Pulse-Shaping Capabilities Using Nested Conical Wire-Array Z-Pinches

D. J. Ampleford, S. N. Bland, M. E. Cuneo, S. V. Lebedev, D. B. Sinars, *Member, IEEE*, C. A. Jennings, E. M. Waisman, R. A. Vesey, G. N. Hall, F. Suzuki-Vidal, J. P. Chittenden, *Member, IEEE*, and S. C. Bott, *Member, IEEE*

***Abstract*—We present data from experiments using nested wire-array Z-pinches where the wires of one of the arrays (the outer or inner array) are inclined to produce a cone. The use of these nested conical arrays can potentially provide a valuable tool in X-ray radiation pulse shaping for Z-pinch-driven high-yield inertial-confinement-fusion schemes. Conical nested arrays can produce a zippered implosion which broadens the main radiation pulse and, possibly, the pulse associated with the interaction of the two arrays. Results from experiments at current levels of 1 MA (240 ns) and 18 MA (100 ns) are presented and compared. Experiments at 1 MA with a conical outer array indicate broadening of the full-width at half-maximum of the main stagnation radiation pulse, with results at 20 MA showing a similar result. Conical inner arrays do not broaden the main radiation pulse because a longer inner array ablation time offsets the earlier interaction time of the outer array with the inner array. Although array dynamics data suggest that a conical inner or outer array can potentially provide control of the interaction radiation pulse, this was not observed. Observations are consistent with a wire-array trajectory model incorporating outer and inner array ablation, snowplow physics, and a simplified array interaction model.**

***Index Terms*—Plasma measurement, plasma pinch, X-ray measurement.**

I. Background

WIRE ARRAY Z-pinches are an extremely powerful ($\sim$200 TW) laboratory X-ray source and have been explored as a potential driver for inertial confinement fusion (ICF) [1], [2]. One strict requirement for any ICF capsule driver is the ability to shape the X-ray drive pulse to implode the capsule on a low adiabat and minimize the energy required for fuel compression [3]. For Z-pinch-driven ICF, it is possible to engineer the wire array in order to create this pulse. Many pulse-shaping tools have previously been developed using nested wire-array Z-pinches [1], [4] and with foam targets on axis [1]. Specifically, utilizing the interaction pulse as the outer array passes the inner array and the radiation pulse generated as plasma first collides with a CH foam on axis prior to fully collapsing to provide a "foot pulse" and a "first step" is discussed below [1].

Fig. 1 shows the controls that are required in order to achieve ignition and high-yield fusion [5]. Control is needed of the intensity and duration of the foot pulse (T_{foot} and τ_{foot}, respectively). For the Z-pinch pulse-shaping scheme described by Cuneo *et al.* [1], this is achieved using the interaction of the outer array material with the inner array. Next, control is needed of the intensity and timing of the first step (T_{first} and τ_{first}, respectively), which is achieved by the interaction of the imploding material with an on-axis foam. Finally, control is needed of the timing and duration of the main peak (T_{main} and τ_{main}, respectively). Ideally, control over these requirements could be achieved independently with different parameters. Previous data have demonstrated the good control of the radiation pulse shape, approaching the necessary controls required to achieve ignition [1]. One notable exception is that the pulse length of the main pulse is too short [1]; a temporal compression of electrical energy into the load to the stagnation radiation pulse of 40:1 is achieved with nested arrays, with a full-width at half-maximum (FWHM) of the stagnation pulse as short as 2.5 ns. While future longer-rise-time generators may achieve a similar compression ratio, and hence a longer main pulsewidth, it is desirable to have an independent control of the FWHM. Here, we investigate the added control achieved by tapering one or both of the nested wire arrays, to produce conical nested arrays.

The implosion time of a wire-array Z-pinch is strongly dependent on the array diameter (along with the mass, current pulse, and many other factors) [6]. This can be seen by simply considering that the implosion time τ_{imp} is proportional to mr_0^2 [6], where m is the mass per unit length of the array and r_0 is the array radius. If r_0 is varied with axial position z (as is the case in a conical wire array), the implosion time will

Manuscript received May 1, 2012; revised July 28, 2012 and September 5, 2012; accepted September 12, 2012. Date of publication November 15, 2012; date of current version December 7, 2012. This work was supported in part by the SSAA program of the NNSA under DOE Cooperative Agreement No. DE-FC03-02NA00057. Sandia National Laboratories is a multiprogram laboratory managed and operated by Sandia Corporation, a wholly owned subsidiary of Lockheed Martin Corporation, for the U.S. Department of Energy's National Nuclear Security Administration under Contract DE-AC04-94AL85000.

D. J. Ampleford, M. E. Cuneo, D. B. Sinars, C. A. Jennings, E. M. Waisman, and R. A. Vesey are with the Sandia National Laboratories, Albuquerque, NM 87185 USA (e-mail: damplef@sandia.gov; mecuneo@sandia.gov; dbsinar@sandia.gov; cjennin@sandia.gov; emwaism@sandia.gov; ravesey@sandia.gov).

S. N. Bland, S. V. Lebedev, G. N. Hall, F. Suzuki-Vidal, and J. P. Chittenden are with The Blackett Laboratory, Imperial College London, SW7 2BW London, U.K. (e-mail: sn.bland@imperial.ac.uk; s.lebedev@imperial.ac.uk; gareth.hall@imperial.ac.uk; f.suzuki@imperial.ac.uk; j.chittenden@imperial.ac.uk).

S. C. Bott is with the Center for Energy Research, University of California San Diego, La Jolla, CA 92093 USA (e-mail: sbott@ucsd.edu).

Color versions of one or more of the figures in this paper are available online at http://ieeexplore.ieee.org.

Digital Object Identifier 10.1109/TPS.2012.2222051

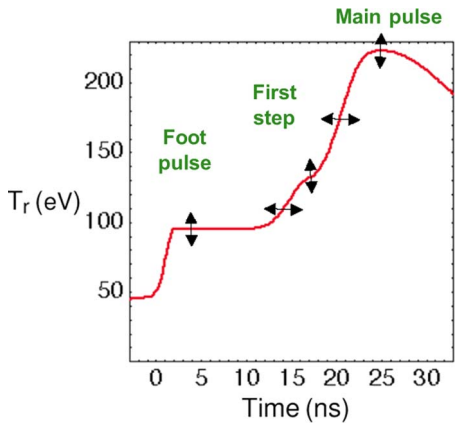

Fig. 1. Temperature profile needed for ignition and high yield with the double-ended hohlraum [5]. Control of the timing, intensity, and duration of the foot pulse, the first step, and the main pulse.

also vary as a function of z, leading to a zippered implosion and temporally longer X-ray pulse. This will be true even with wire ablation, as is demonstrated hereinafter using a snowplow implosion model. Gas puff Z-pinches often experience an axial zipper through axial variations in both the mass per unit length and the radial density distribution. In a conical array, different axial locations have different effective radii $(r = r(z))$, and this will alter the implosion time of these different axial positions, thus temporally spreading the emitted X-ray pulse. Previous work on conical wire arrays has utilized this configuration to model astrophysical jets [7]–[12] or, more recently, to study the implosion dynamics of single conical arrays [13], [14]. Imploding single conical array experiments have demonstrated the utility of conical arrays to broaden the main radiation pulse [14].

In this paper, we extend previous work to study the implosion dynamics and radiation pulse-shaping capability of nested conical wire arrays in a nested wire-array configuration. In the next section, we discuss experimental setups and described predictions of changes to the pulse shape. Following this, we described experiments with a conical outer array and, then, with a conical inner array. Finally, we summarize by comparing the predictions made in the next section to the experimental data.

II. Description of Experiment

A. Experiments on the Z Facility

Nested wire-array implosion dynamics are more complex than single wire arrays, with inductive and resistive current distribution between the arrays [1], [4] and the potential for the arrays to pass each other semitransparently [4], [15], [16]. Here, we investigate whether a modification of the nested wire array, where the wires of one of the arrays (outer or inner) are inclined with respect to the axis, can be used to control the radiation pulse shape from a nested wire array. The wire-array setups used on the Z generator consist of a conical outer array with a cylindrical inner array, a cylindrical outer array with a conical inner, and the standard cylindrical outer and inner arrays, as shown in Fig. 1. The anode and cathode diameters

TABLE I
Experimental Setup for Conical Nested Shots on Z. All Wire Arrays Are 10 mm Tall

Shot number	Z1560	Z1639	Z1574
Configuration	Standard	Conical outer	Conical inner
Outer Anode diameter	20mm	20mm	20mm
Outer Cathode diameter	20mm	22mm	20mm
Inner Anode diameter	12mm	12mm	12mm
Inner Cathode diameter	12mm	12mm	10mm
Return can diameter	30mm	32mm	30mm

of the outer and inner arrays are specified in Table I. For all shots, the anode configuration is kept the same, with a 20-mm anode diameter, identical to the standard compact array setup described by Cuneo *et al.* [1]; however, the cathode diameters are altered to create the conical arrays. All wire arrays are 10-mm-tall nested wire arrays, consisting of 300 wires, each 7.3 μm in diameter, in the outer wire array and 30 wires, each 16.6 μm in diameter, in the inner wire array. The feed gap between the cathode and the return current can is kept at 5 mm in all shots (leading to a larger return current can for shot Z1639).

We now describe the predictions of what the presence of conical outer or inner wire arrays will do to the radiation pulse from a nested wire array. To a first approximation, the implosion time of each axial location in a nested conical array will follow the trajectory of a cylindrical nested array with the initial radii identical to the initial radial locations of that position in the conical array. The Array On Array ABLation (AOABL) snowplow model coupled to a circuit model for the Z generator [17]–[19] configured to represent a nested array configuration [1] has been used to estimate the implosion trajectories of cylindrical wire arrays equivalent to the anode and cathode ends of the nested configuration shown in Fig. 2(b) and (c). The details of the AOABL model are given in the Appendix.

We chose snowplow model input parameters identical to those demonstrated by Cuneo *et al.* [1] to provide a good fit to cylindrical nested array implosion trajectory measurements. These are an ablation velocity $v_{abl} = 20$ cm/μs and the conditions that 50% of mass is ablated prior to the start of implosion, 18% of mass remains at the initial location as trailing mass, and 30% of the outer array momentum is transferred to the inner during the interaction. These input parameters have been kept fixed for the four trajectories discussed hereinafter.

Fig. 3(a) and (b) shows the results of snowplow calculations for the conical outer and conical inner setups, respectively, for the Z experiments. At the top of each graph (red curves) the trajectories of the outer and inner arrays for the configuration equivalent to the cathode of the array are plotted, and at the bottom, the trajectories for the arrays equivalent to the anode are plotted (blue curves). For this figure, we have independently calculated the expected implosion trajectories as if the entire outer wire array had the diameter used at the cathode and as if the entire wire array had the diameter used at the anode. This treatment allows the circuit to react differently to the different section of the array, rather than providing a self-consistent model of the zippered implosion. This treatment is sufficient to demonstrate the dependence of the trajectory on the initial wire locations. Ideally, a full representation of the conical array

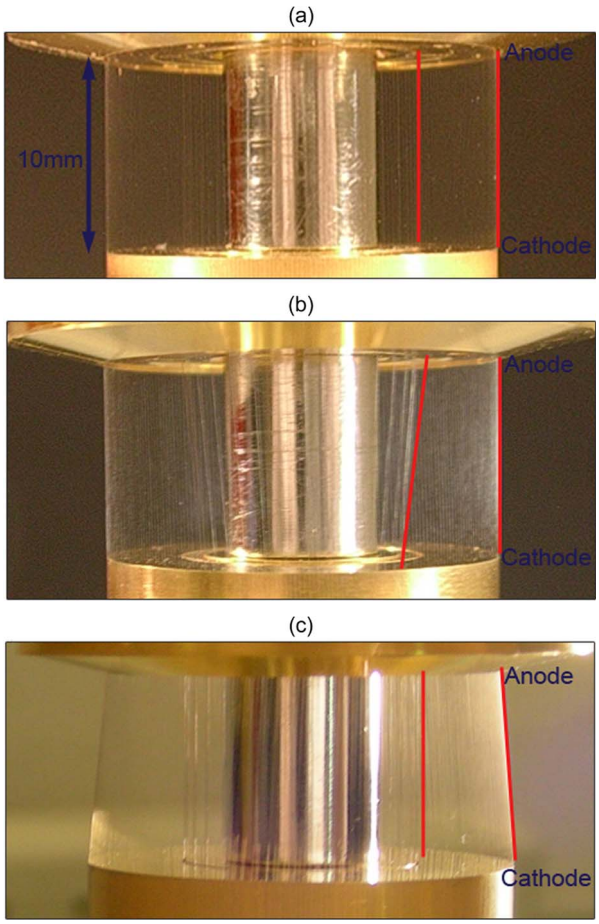

Fig. 2. Preshot photographs of nested arrays on Z with (a) standard array (e.g., Z1560), (b) conical inner array (Z1574), and (c) conical outer array (Z1639) configurations. The anode (A) is at the top of each of the images, and the cathode (K) is at the bottom, as shown. The metal object on the center of each array is an installation rod which is removed after the installation of the array in Z. See Table I for array dimensions. (a) Z1560: Cylindrical outer on cylindrical inner. (b) Z1574: Cylindrical outer on conical inner. (c) Z1639: Conical outer on cylindrical inner.

would be calculated, and the inductance at each time step would be used to determine the drive current. It is noted that, in the actual experiments, a low-density foam is fielded on the wire-array axis to add additional pulse-shaping capabilities—to simplify, this is omitted from the current discussion.

In the conical outer case [see Fig. 3(a)], the arrays interact (pass each other) at ∼190 ns. The variation between the two ends of the array interacting is designated in the plot by a hashed region. Due to the lower initial magnetic field strength near the cathode and larger distance to travel, the interaction here is almost 5 ns later than that at the anode. As the arrays move to smaller radii, this time lag is diminished; however, it remains almost 3 ns at stagnation (shown by a cross hashed region on the plot).

For the conical inner case [see Fig. 3(b)], the trajectories are identical for the outer arrays equivalent to the anode and cathode; however, the different positions of the inners lead to a difference of ∼3.5 ns in the time that the arrays pass each other (again shown by a single hashed region). This variation in the trajectory is diminished after the interaction due to the difference in the distance between the inner array and the axis

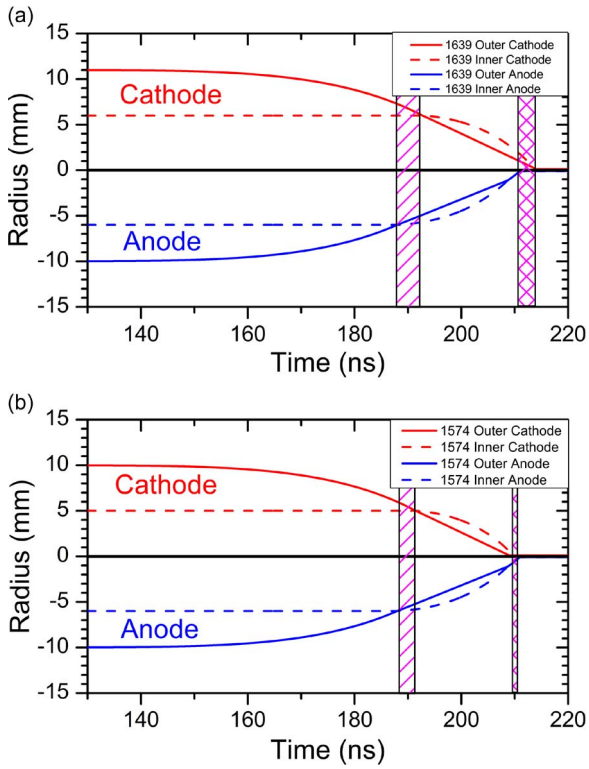

Fig. 3. Estimates of the trajectory with (a) a conical outer array and (b) a conical inner array on the Z generator. The model is using an ablation velocity $v_{abl} = 20$ cm/μs and the conditions that 50% of mass is ablated prior to the start of implosion, 18% of mass remains at the initial location as trailing mass, and 30% of the outer array momentum is transferred to the inner during the interaction. Vertical boxes on each plot represent the time difference between the anode and the cathode end reaching the (single hashed) inner array and (cross hashed) axis. (a) Z1639: Conical outer. (b) Z1574: Conical inner.

at each end; however, it remains at a level of almost 2 ns at stagnation (cross hashed).

Hence, we see that using a conical array as either the inner or the outer array of a nested array will have an effect on the stagnation time of different locations in the arrays and is hence likely to lengthen the emitted X-ray pulse. It is noted that this change Δt in the stagnation or interaction time for different regions of the array will not directly lengthen the FWHM τ of the appropriate pulse by Δt. Instead, the pulse emitted by the cylindrical array (which is approximately Gaussian) of width τ should be convolved with the zippering of the stagnation, leading to an FWHM for the conical case (τ_{con}) which can be approximated as

$$\tau_{con} \approx \sqrt{\tau_{cyl}^2 + (f_v \Delta t)^2} \tag{1}$$

where f_v is the fraction of the pinch viewed by the diagnostics. Hence, for the conical outer case, the FWHM of the stagnation pulse is expected to be ∼2.9 ns, compared to the standard 2.5 ns from a cylindrical outer array (with the view factor f_v being half of the pinch for both cases).

Diagnostics employed in the Z experiments included X-ray self-emission imaging at $>$ 1.185 keV, radiography at 6.151 keV, diamond photoconducting diodes (PCDs [20]) and X-ray diodes (XRDs [21]), and bolometers [22].

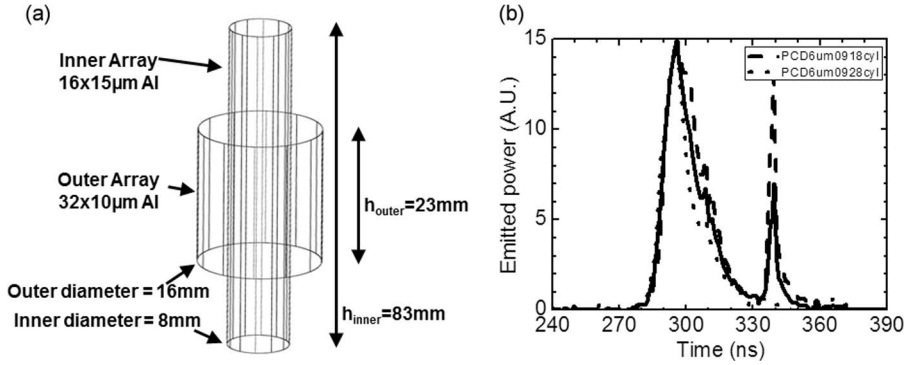

Fig. 4. (a) Setup for high-inductance inner on MAGPIE. (b) (Dotted lines) Comparison of two nested array shots on MAGPIE and (solid line) the average of these shots.

B. Experiments on MAGPIE

In addition to the experiments on the Z generator at Sandia National Laboratories (20 MA, 100 ns [23]), experiments were also performed on the MAGPIE generator at Imperial College London (1 MA, 250 ns [24]). In general, the use of smaller $\sim$1-MA university-scale generators provides a platform to explore new concepts in greater depth, allowing a high number of well-diagnosed experiments to be performed. Specifically for these experiments, the use of MAGPIE allows better diagnosis of the plasma from the initial wire positions to the axis, without being obscured by current return posts, and with diagnostics such as extreme UV (XUV) self-emission imaging ($h\nu >$ 30 eV) that are well suited to diagnosing the implosion of the plasma over the full evolution from immediately following wire initiation through to stagnation onto the axis. While different machines allow the use of additional diagnostics, Z and MAGPIE have different characteristics, including a difference in rise time (100 ns versus 250 ns) and peak current (20 MA versus 1 MA). In order to scale results and interpretations from 1-MA machines to larger facilities, care must be taken that the same physics is being observed on both machines. For nested wire arrays, two key parameters that dictate the dynamics of the system are the initial division of current between the two arrays (fraction of current through the inner array) and the transparency of the inner array as the outer implodes past the inner [1], [4]. These two factors are, in fact, related, as the dynamics of the inner array (e.g., core size and ablation) are dictated by the level of current flowing through it. This current fraction through the inner array at a given time is determined by two factors: At very early times, the ratio of the resistances is important; however, at later times, the ratio of the inductances of the inner and outer arrays dictates the current distribution [4].

The tungsten nested wire arrays used in the double-ended hohlraum on the Z generator utilize high wire numbers in the outer array. This high wire number leads to a much lower inductance of the outer array compared to that of the inner array ($L_{out} \ll L_{in}$), leading to the inner being inductively screened by the outer. Based on inductive current division, the majority (99%, 5.7 MA at 40 ns) of the current passes through the outer array, while the inner array experiences negligible current (1%, 45 kA) [4].

It is possible to engineer wire arrays such that a similar inductive difference is present with lower-outer-wire-number arrays on 1-MA generators, as discussed by Bland *et al.* [4]. Experiments on MAGPIE have shown that lengthening the inner array [as shown in Fig. 4(a)] compared to the outer array can enhance the inductive contrast between the arrays [4], reducing the current through the inner array to a negligible level (as verified by B-dot probes, radiography, and the trajectory of the arrays measured by radial optical streak photography [4]). Data such as that shown in Fig. 4(b) indicate that this setup can have good shot-to-shot reproducibility through the main X-ray pulse despite the relatively low wire numbers used.

Using the high-inductance inner configuration on MAGPIE transforms the conical nested configurations from those shown in Fig. 2 to those shown in Fig. 5. In contrast to the tungsten wire arrays used in the Z experiments, the MAGPIE experiments use aluminum wire arrays. All MAGPIE experiments discussed here utilize an outer array of 32 wires, each 10 μm in diameter, and an inner array of 16 wires, each 15 μm in diameter, with an outer-wire-array diameter of 16 mm and an inner-wire-array diameter of 8 mm. To provide comparisons to Z data, the angles of the conical arrays are kept the same as for the Z experiments. On MAGPIE, the conical outer case uses a smaller diameter at the cathode compared to the smaller diameter anode used on Z. Assuming that MHD effects dominate the implosion dynamics, this should not severely impact the implosion. We note that the previously observed cathode end effects [25] are not observed in any of the experiments discussed here.

To diagnose the MAGPIE experiments, laser shadowgraphy, time-resolved XUV ($>$ 30 eV) emission imaging [26], PCDs, and XRDs were fielded. In addition, two diagnostics have been developed on MAGPIE specifically for these experiments to provide information on axial variations in the pinch, particularly the time of stagnation onto the axis at different axial positions. The imaging system of a radial optical streak camera has been configured to split the relayed optical image and demagnify it such that two images can be located on the same streak camera photocathode, allowing simultaneous streak photography at multiple axial locations. The setup for this is shown in Fig. 6(a)—the anode of the nested wire array is imaged onto the left side of the streak camera slit (shown in red) while the cathode of the wire array is imaged onto the right side of the streak camera slit (shown in blue). This allows one streak to capture two different regions of the implosion on the same timescale, with the same magnification. Additionally, an

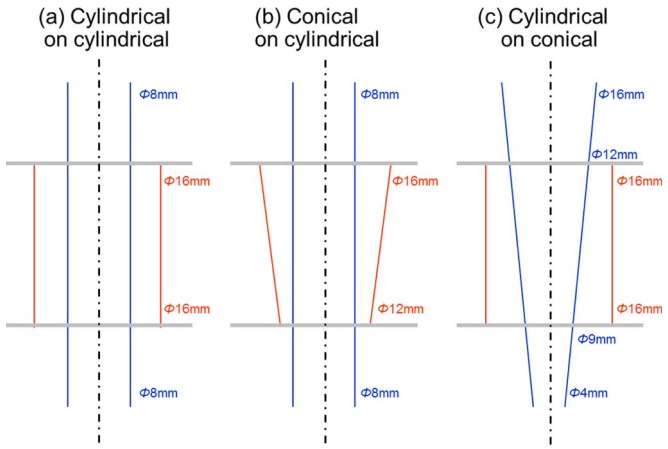

Fig. 5. (a) Nested array setup on MAGPIE using a long inner array to limit current through the inner array. (b) Nested array with conical outer. (c) Nested array with conical inner. For all shots, the outer array is 23 mm tall, and the inner array is 83 mm tall. (a) Cylindrical on cylindrical. (b) Conical on cylindrical. (c) Cylindrical on conical.

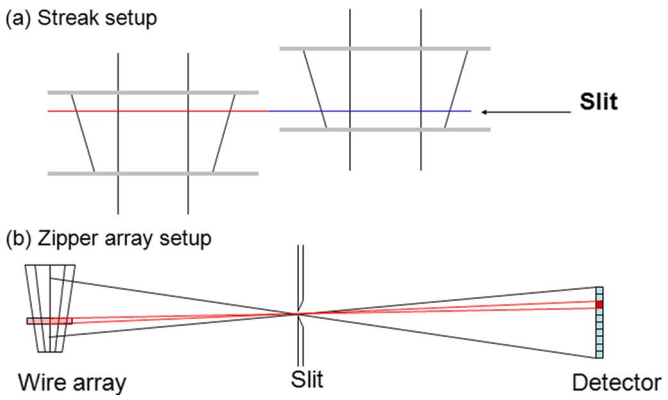

Fig. 6. (a) Setup of optical streak camera with radial resolution, where multiple images of the array are projected onto the streak camera enabling the recording of streak images at two different axial positions. (b) Si-diode zipper array setup, where a horizontal slit is used to image the emission of the array onto a vertical Si-diode array, providing axially resolved emission measurements.

axially resolved Si-diode (zipper) array has been developed. A horizontal slit is used to produce an axial image of the pinch onto a 12-element silicon photodiode array (International Radiation Detectors AXUV-10EL silicon photodiode). This is shown in Fig. 6(b). As seen from the figure, this instrument inverts the image onto the image plane—when we discuss the data from this zipper array later, we refer to the regions where the emission originated. We note that, for debris mitigation, this zipper array utilizes a different filtering combination than the PCDs, resulting in the zipper array sampling a higher photon energy band (> 1 keV for the zipper array and > 200 eV for the PCDs).

III. Results With Conical Outer Wire Array

The first experimental setup that we consider consists of a conical outer wire array and a cylindrical inner wire array. In a wire array, the mass ablation rate has been determined to vary with magnetic field and, hence, for a given current, to vary with the radial location of the wires [27]. Table I shows the details of the wire-array setups being used. The mass ablation rate of the conical outer of a nested array configuration varies along the length of the wire, as has previously been shown with single conical wire arrays [14]. This results in an axial dependence of the time that the wire material becomes depleted and the array begins to move. For MAGPIE, the smaller diameter cathode implodes first followed by a steady zipper in the start time of the implosion to the anode (for Z, it will be the smaller diameter anode that will start to implode first). The zippered wire breakage is seen experimentally in Fig. 7; by 220 ns, the cathode of the array has begun to implode. In the following frames, the other axial positions begin to move, and by the final frame (235 ns), the full length of the outer array is in motion. The axial location of the wire breakage seen in each frame of Fig. 7 is consistent with [14, eq. (6)].

Diagnosing the time that the outer wire array meets the inner wire array provides an independent measurement of how the interaction pulse will vary with different setups. On MAGPIE, the interaction pulse is not observed due to relatively high asymmetries resulting from the moderate wire numbers used. Over the 15 ns sampled in this figure, the interaction location has moved by 6.7 mm; hence, it is likely to take $\sim$50 ns for the interaction to zipper from the base of the inner array to the top. We speculate that this could result in a longer interaction pulse than for the standard cylindrical nested wire-array case; however, we note that it is likely that the energy radiated in the interaction pulse would remain constant, leading to a decrease in the peak power of the interaction pulse.

Following the interaction of the outer with the inner array, the inner array undergoes an ablation phase. The zippered interaction of the two arrays seeds an axial variation in the evolution of the inner array, with the inner array beginning to implode first near the cathode, followed by a steady axial zipper from the cathode to anode. Fig. 8 shows XUV self-emission images from the imploding inner at four different times. The images show a steady zipper in the implosion, which, in 10 ns, changes the axial position by 13.9 mm (for a given side of the array). The zipper of the array onto the axis results in different regions of the array emitting at different times. This XUV image also indicates that there is some asymmetry between the two sides of the array, with the left side proceeding the right side by $\sim$800 μm. While this will have an effect on the X-ray pulse, this is only responsible for an $\sim$6-ns lengthening, whereas the axial variation is equivalent to 16.5 ns [based on (1)]. On MAGPIE, this zipper starts at the smaller initial diameter end of the array, the cathode. Again, we note that, on Z, the smaller end of the array is the anode; hence, we expect the direction of the zipper to be reversed.

Fig. 9(a) shows the results of radial optical streak cameras for the cylindrical-on-cylindrical and conical-on-cylindrical experiments. For each of these setups, the camera samples at two distinct locations in the array [approximately 1/3 and 2/3 of the way between the electrodes; see Fig. 6(a)]. These data are in agreement with Fig. 8, indicating an axial variation in the time that the implosion reaches the array axis.

The axial zipper array data, shown in Fig. 9(b) for the conical outer array and standard nested wire-array cases on MAGPIE,

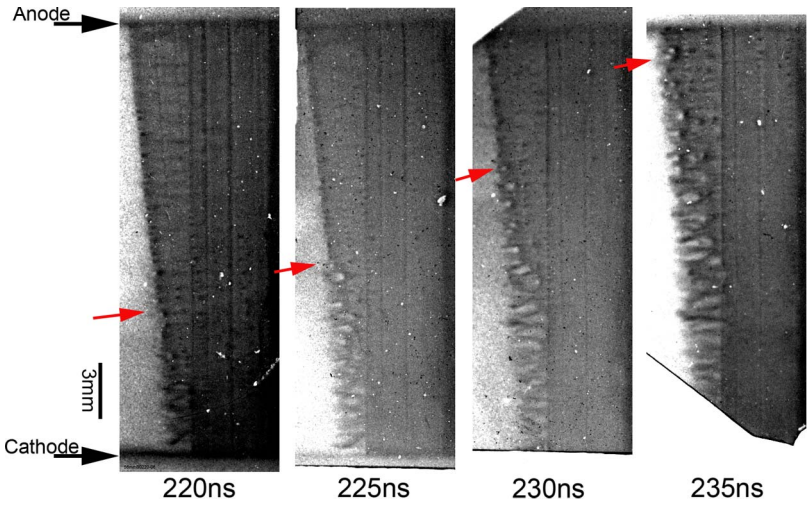

Fig. 7. Time-gated XUV emission images of one side of the conical nested array on MAGPIE. Outer wires are seen to break at axially dependent times (as indicated with red arrows). As a result, the time of interaction of the outer with the inner also varies with axial position.

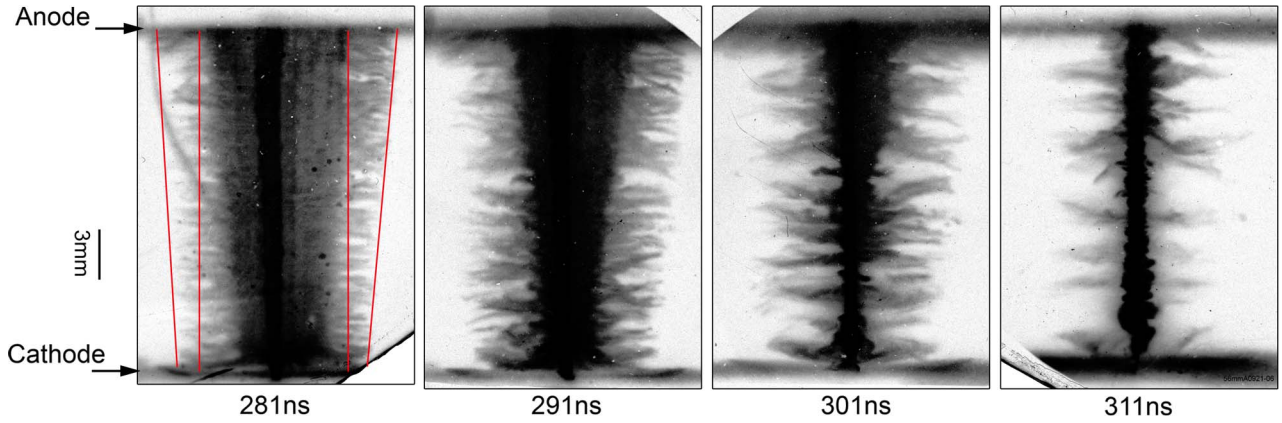

Fig. 8. XUV emission for a nested array with a conical outer array indicates that a zipper is present in the implosion after the inner begins to implode. For MAGPIE, due to low wire numbers used, a left–right asymmetry is seen in the data. The initial positions of the outer and inner wire arrays are shown on the first frame.

illustrate how the axial variation in implosion time affects the X-ray pulse. For the cylindrical outer case, the different regions of the array emit at very similar times ($\sim$5 ns random variation in timing); however, for the conical outer case, a steady zipper is present along the length of the array, with a 30 ns variation between the elements of the zipper array viewing the highest and lowest extents of the wire array. Comparison to the PCD signals [see Fig. 9(c)] shows that the zipper relates directly to a change in the length of the X-ray pulse for the two configurations. The zipper array is only sampling $\sim$70% of the length of the pinch while the PCD signal in Fig. 9(c) integrates the complete length of the pinch and hence shows a slightly wider X-ray pulse.

The difference between these PCD signals is shown in Fig. 10(a), which shows an overlay of the signals for conical and cylindrical outer arrays. The PCD in each case is filtered with 1.5-μm polycarbonate, providing the transmission of photon energies > 250 eV. It is clear from the plot that the conical outer has a longer rise time (24 ns compared to 11 ns) and a longer pulse length (FWHM is 30 ns compared to 15 ns). The peak power has also dropped by 25% while the total radiated yield has increased by 30%.

For the conical outer array on MAGPIE, the zipper array, axially resolved stream, and radiated X-ray pulse are consistent with each other, each indicating that the zipper from the cathode to anode takes $\sim$30 ns.

A similar nested array configuration, with a conical outer, has been fielded on Z (shot Z1639). This setup consisted of an outer array with the diameter varying from 20 to 22 mm and a 12-mm-diameter inner array. The inner and the outer array both had masses of 2.5 mg, with 300 wires in the outer and 30 in the inner (as used by Cuneo *et al.* [1]). The anticipated trajectories of the two ends of this array were displayed in Fig. 3, showing an expected 2.85 ns difference in the stagnation time of the two ends of the array.

Fig. 11(a)–(d) shows the X-ray framing camera images of the stagnation of the nested array with a conical outer on Z. The data show a clear zipper in the stagnation, with the anode (top of the image), which initially had a smaller outer diameter, starting to stagnate by -2.3 ns. This is followed by the center of the pinch stagnating during the following frame (-0.3 ns) before, finally, the cathode region is stagnating by $+1.7$ ns to 3.7 ns. This contrasts to Fig. 11(e), which shows that, for a standard cylindrical nested array, the entire length of

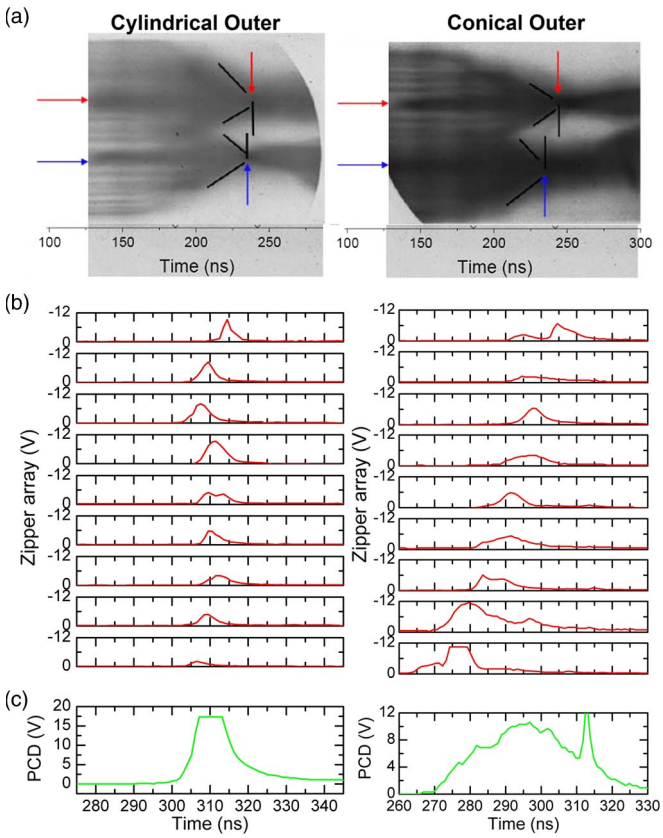

Fig. 9. (a) Streak showing stagnation time variation for outer conical and cylindrical configurations. (b) Results of a zipper array for nested array experiments with cylindrical and conical outer arrays, each with a cylindrical inner [b is a slightly different array configuration to part (a)]. The zipper array plots correspond to diodes viewing different regions of the pinch, with the upper plot corresponding to a region near the anode of the array and the lower plot corresponding to a region near the cathode of the array (refer to Fig. 6(b) for more details). (c) PCD signals for the same shots as (b), viewing the full length of the array (the plot on the left is clipped). (a) is for a different array configuration than (b) and (c); hence, the timescale of that part does not match the remainder of the figure.

the pinch is radiating at peak power, rather than as a zippered stagnation. As with the data on MAGPIE, this imposed zipper should lead to a lengthening of the radiation pulse emitted by the array compared to a cylindrical nested array, where no zippering is present, as was shown in Fig. 3. Fig. 10(b) shows a comparison of the X-ray pulses with and without this tapering of the outer array. The plot shows that, as would be expected, the stagnation is temporally stretched. A comparison shows that the FWHM of the main pulse is increased from 2.5 to 2.93 ns. There is a small drop in the peak power associated with this broadening of the X-ray pulse; however, the total radiated energy is actually increased. In the plot, the interaction pulse [at 65 ns in Fig. 10(b)] is seen to have a higher magnitude with the conical outer array than with the cylindrical outer. We believe that this is due to the initially larger diameter of the cathode region of the array; it has previously been shown that larger diameter arrays have a larger interaction pulse associated with them [4]. The data here indicate that there is no significant change in the duration of the interaction pulse. While Fig. 3 indicated that there should be a few nanoseconds of change in time of the array interaction between the anode and cathode, this is small compared to the 5-ns length of the interaction

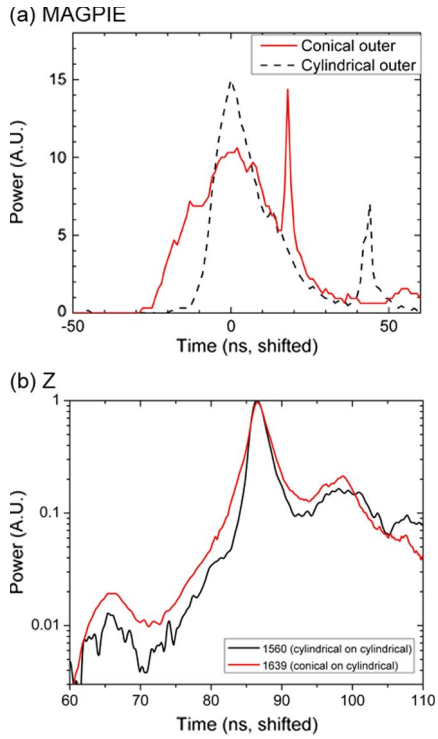

Fig. 10. Comparison of (a) PCD signals on MAGPIE and (b) XRD power pulses on Z for nested arrays with conical (Z1639) and cylindrical (Z1560) outer arrays, each with a cylindrical inner array. Waveforms have been time shifted such that the peak powers coincide.

pulse in a standard nested wire array; the convolution [see (1)] of the imposed zipper with the interaction pulse timescale is almost identical to that of the original interaction pulse (we expect a new interaction pulse length with the conical outer of 5.5 ns).

These results [see Fig. 10(b)] are generally in agreement with the MAGPIE data [see Fig. 10(a)], indicating a significant temporal broadening of the main X-ray pulse.

IV. Results With Conical Inner Wire Array

Additional experiments utilized a cylindrical outer wire array with a conical inner array. In this configuration, the cylindrical outer array is expected to behave similarly to the outer of a standard nested array until it interacts with the inner array. Specifically, the time of this interaction should vary with axial position due to the difference in distance that must be traveled prior to interaction with the inner array. Fig. 12 shows the XUV self-emission images of a nested array conical inner on MAGPIE. The first of these frames indicates that the outer array has arrived at the position of the inner array near the anode (top of the image). By the second image, the full length of the imploding sheath has passed the inner, and the inner is ablating.

The axial variation in the ablation of the inner array in this configuration acts to compensate for the variation in the time that the outer array reaches it. The current is switched first into the inner array nearest the anode; however, because of the lower magnetic field strength at this position, once the current has switched into the full length of the wire, the mass ablation is

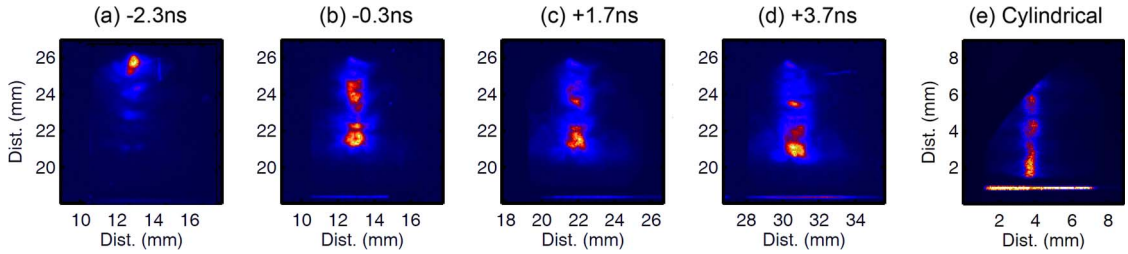

Fig. 11. Time-resolved X-ray imaging on Z with a conical outer array using a 5-μm Parylene-N filter (200–300 eV), at times (a) -2.3 ns, (b) -0.3 ns, (c) $+1.7$ ns, and (d) $+3.7$ ns relative to peak X-rays. Also shown, (e) is one frame from a cylindrical-on-cylindrical nested array, which does not show the extreme zippering seen in (a)–(d).

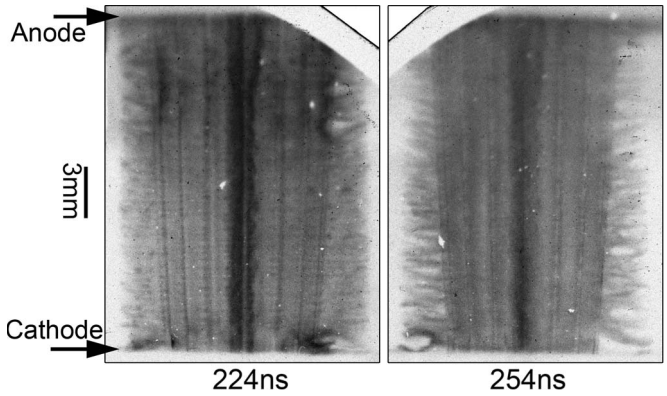

Fig. 12. XUV emission imaging with a conical inner array shows that the implosion of the outer is axially uniform; however, the time that it reaches and interacts with the inner varies with the radial position of the inner, which varies along the length of the array, at 224 and 254 ns.

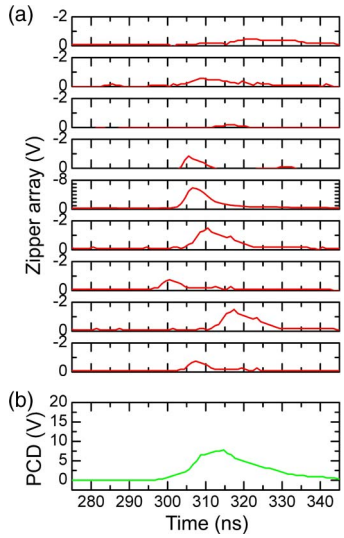

Fig. 13. (a) Result using a zipper array for a cylindrical-on-conical nested array. The zipper array plots correspond to diodes viewing different regions of the pinch, with the upper plot corresponding to a region near the anode of the array and the lower plot corresponding to a region near the cathode of the array (refer to Fig. 6(b) for more details). (b) PCD pulse shape for cylindrical outer array and conical inner array, which can be compared to the plots in Fig. 9(c).

fastest near the cathode. The overall result of the ablation and start of the inner array implosion results in an axially uniform stagnation (i.e., not zippered), as seen in Fig. 12. We note that, although the wire ablation process is qualitatively similar between MAGPIE and Z with steady ablation of material from the wire cores, quantitatively, the ablation time is different with $\sim$5–6 ns wire ablation typical of experiments on Z [1] and $>$ 50 ns typical of experiments on MAGPIE [4].

As was shown in Fig. 3, with the conical inner array, we do not expect a significant zipper to be present when the array stagnates onto the axis. The zipper array data for the conical inner experiment on MAGPIE, shown in Fig. 13, indicate that there is no trend in the time of the material reaching the axis; hence, after the ablation of the inner array, the axial variation in the implosion has been minimized. We note that there is an indication that there may be more random variation in the stagnation time than for a cylindrical-on-cylindrical array, as is seen by comparing Fig. 9(a) with Fig. 13. Data in this cylindrical-on-conical nested configuration on MAGPIE [see Fig. 14(a)] show a similar pulse length to that of cylindrical-on-cylindrical arrays; however, the total energy output is lower. Both laser imaging and time-integrated self-emission imaging indicate that this could be the result of the largest diameter section of the inner array not imploding during the current pulse, hence reducing the length of the pinch emitting by $\sim$20%–30%.

For Z, radiography data are available that show the mass distribution prior to stagnation. Fig. 15 shows the radiographs of two nested arrays, one with a conical inner and one with a cylindrical inner array obtained using monochromatic backlighting with the Z-beamlet laser [28].

For the cylindrical-on-cylindrical case, the axial variation in the radial position of the sheath is ≤ 100 μm. In the radiograph for the conical inner, there is an $\sim$300 μm variation in the location of the imploding sheath from the top to the bottom of the 4-mm field of view. At a typical implosion velocity of 30 cm/μs [1], this is equivalent to an $\sim$2-ns zipper along the 10-mm pinch length, which is consistent with the predictions of Fig. 3. Applying (1) indicates that we expect a lengthening of the pulse within the field of view of the XRDs of 0.19 ns.

Fig. 14(b) shows the radiated power pulse for a nested array with a conical inner on Z (shot 1574). As with the conical outer case, we expect there to be a zippering of the interaction of the outer and inner arrays; however, due to the already long interaction pulse for nested arrays on Z ($\sim$5 ns), it does not significantly lengthen the timescale of the radiated interaction pulse. The FWHM of the main pulse is 0.2 ns more than the cylindrical case. The impact of the interaction time of the outer with the inner array and the ablation time of the inner array

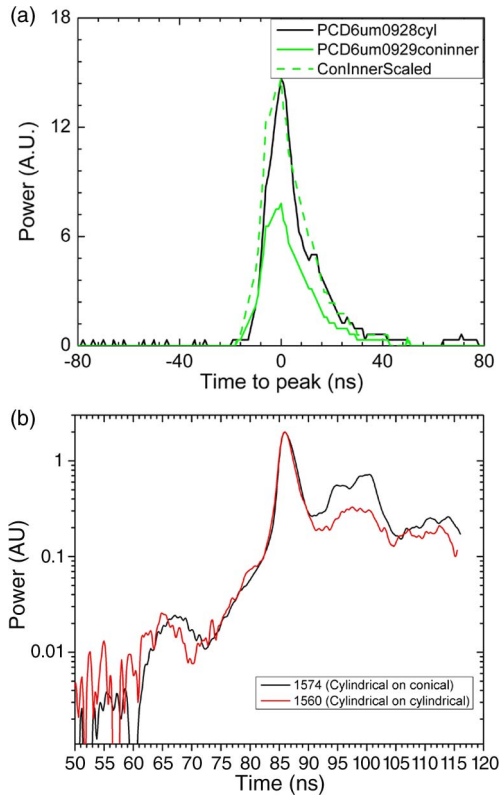

Fig. 14. (a) MAGPIE and (b) Z power pulses comparing cylindrical-on-conical to cylindrical-on-cylindrical nested arrays. There is no change in the main pulse using the conical inner; however, the first step appears less pronounced.

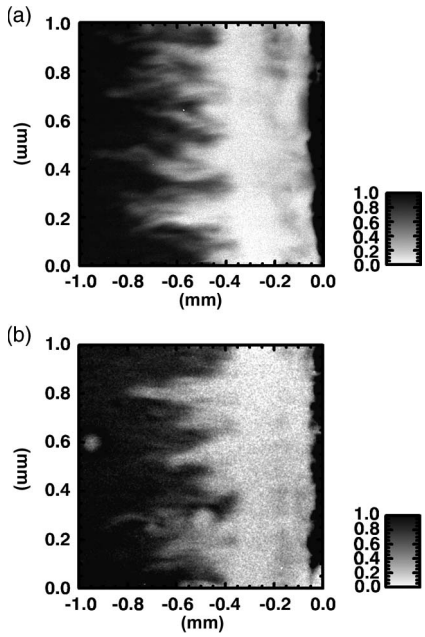

Fig. 15. Z radiography of shots Z1574 (cylindrical on conical) and Z1560 (cylindrical on cylindrical) shows negligible difference in mass distribution prior to stagnation for the conical inner case. The axis of the array is at $x = 0$. Self-emission is seen on the axis of the pinch. A transmission scale is shown—black is full transmission, and white is full absorption. (a) Z1574 conical inner. (b) Z1560 standard inner.

appear to offset each other, as was seen on MAGPIE. The effect of the conical inner array is less significant than that of the conical outer array as shown in Fig. 10. We note that

TABLE II
DATA FOR Z NESTED SHOTS WITH A COMBINATION OF CONICAL AND CYLINDRICAL OUTER AND INNER ARRAYS. ALL ARRAYS HAVE 2.5 mg IN THE OUTER ARRAY AND 2.5 mg IN THE INNER ARRAY. CYLINDRICAL ARRAYS HAVE 20-mm OUTER DIAMETER AND 12-mm INNER DIAMETER. CONICAL ARRAYS HAVE THESE DIAMETERS AT THE ANODE AND 2-mm LARGER DIAMETER AT THE CATHODE

Shot number	Z1560	Z1639	Z1574
Outer	Cylindrical	Conical	Cylindrical
Inner	Cylindrical	Cylindrical	Conical
Peak Power	200TW	192TW	198TW
Time of peak power	86.5ns	86.6ns	85.9ns
$f_v \delta t$ from Fig. 3	0ns	2.85ns	1.95ns
$\tau_{calc} = \sqrt{f_v \delta t^2 + \tau_{cyl}^2}$	2.50ns	2.88ns	2.68ns
FWHM (τ_{exp})	2.50ns	2.93ns	2.70ns
Total Energy	1218kJ	1289kJ	1600kJ

TABLE III
DATA FOR MAGPIE NESTED SHOTS WITH A COMBINATION OF CONICAL AND CYLINDRICAL OUTER AND INNER ARRAYS

Shot number	s0918	s0920	s0929
Outer	Cylindrical	Conical	Cylindrical
Inner	Cylindrical	Cylindrical	Conical
FWHM (τ_{exp})	14.9ns	27.4ns	16.0ns

the temporal extent of the lower power emission (at $\sim$10% of the maximum rather than the half maximum) is significantly larger with the conical outer, which is likely associated with a zippered interaction with the on-axis foam. A summary of the X-ray pulse shapes for all three setups on Z is shown in Table II, and that for all three setups from MAGPIE is given in Table III.

V. SUMMARY

We have investigated the use of conical wire arrays in nested configurations as a tool to provide additional pulse-shaping capabilities for Z-pinch-driven ICF. The results demonstrate that the use of an outer conical array and an inner cylindrical array can be used to temporally broaden the stagnation X-ray peak by an amount dictated by the inclination of the cone to the vertical axis. The results are consistent to the first order with a simple array dynamics model that incorporates the ablation and snowplow physics of both the outer and inner arrays, as well as a simplified array interaction model. In the geometry used here, the pulse length was increased by $\sim$50% on MAGPIE, with a gain in total yield. For the specific case presented here, the width at 10% of the peak X-ray power is increased on Z compared to the cylindrical case, likely due to a zippered arrival at the on-axis foam. Interestingly, a conical inner array provided minimal change in the main radiation pulsewidth at both 1 and 20 MA. The longer (shorter) the ablation time of the inner array at larger (smaller) radii offset, to the first order, the earlier (later) the time of interaction of the outer and the inner array at the larger (smaller) radii.

Self-emission imaging data from 1-MA experiments using an outer cylindrical array and an inner conical array suggest that the interaction pulse might be controlled and modified. This was not conclusively proven in this work as no interaction pulse was observed in the 1-MA MAGPIE experiments, and no change to the Z interaction pulse was observed.

TABLE IV
SUMMARY OF CONTROLS ACHIEVABLE USING NESTED WIRE-ARRAY Z-PINCHES, AS PREVIOUSLY DEMONSTRATED BY CUNEO *et al.* [1] AND BLAND *et al.* [4] AND DESCRIBED HERE. 0 DESIGNATES NO DEPENDENCE, 1 DESIGNATES A PRIMARY DEPENDENCE, AND 2 DESIGNATES A SECOND-ORDER DEPENDENCE. "?" IS USED TO IDENTIFY HYPOTHESIZED DEPENDENCES RATHER THAN DEMONSTRATED. THE VARIABLES THAT CAN BE ADJUSTED IN THE ARRAY ARE THE RADIUS, R, AND THE MASS, M, OF THE OUTER OR INNER WIRE ARRAY OR THE ON-AXIS FOAM (DESIGNATED BY $_{outer}$, $_{inner}$, AND $_{foam}$, RESPECTIVELY) OR THE OPENING ANGLE α OF ONE OF THE WIRE ARRAYS. THE VARIOUS PARAMETERS THAT CAN BE CONTROLLED (SHOWN IN THE FIRST COLUMN) ARE SHOWN IN FIG. 1

Feature	R_{outer}	M_{outer}	R_{inner}	M_{inner}	R_{target}	M_{target}	α_{outer}	α_{inner}
τ_{foot}	0	0	1	1	2	2?	2?	1
T_{foot}	1	1	1/0*	0	0	0	0	0
τ_{first}	0?	2?	1	1	1	1?	1	0
T_{first}	0?	2?	1	1	1	1?	1	0
T_{main}	1?	1	1	1	1?	1?	1	0
τ_{main}	1?	1	1	1	1	1?	1	0
Demonstrated by	[4]	[1]	[1]	[1]	[1]	Inferred	Section III	Section IV

The predictability of the present work (e.g., as shown in Table II) suggests that pulse shape controls should be achievable using conical arrays as both the outer and the inner array in a nested configuration, particularly a broadening of the main radiation pulse. As was shown in Fig. 1, variability is required for the intensity and timing/duration of the foot pulse (generated by the interaction of the arrays), the first step (generated by the interaction with an on-axis foam), and the main pulse (generated by stagnation on the axis). Ideally, these six parameters could be controlled with different and independent aspects of the nested array and foam setups. Table IV shows the present status of controls of these six pulse shape parameters through variations in the nested wire array and foam setup. This table incorporates previous work studying how varying the mass and diameter of the outer array, inner array, and foam can be used to control the pulse shape. Combining the present and the previous work, many of these controls of the radiation pulse from a nested wire-array Z-pinch have now been established.

APPENDIX

The array on array ablation is a model to calculate the infinitely thin shell trajectories for nested inner and outer wire arrays. It is self-consistently coupled to the driving circuit, for instance, of the Z machine. AOABL provides the instantaneous load inductance needed to solve the circuit equations. In the version employed in this paper, only the outer array undergoes the ablation and snowplow phases, while the inner array mass is assumed not to vary.

A. Array on Array Inductance, Dynamics, and Momentum Exchange Model

The equations below give the forces driving the array-on-array configuration [29]

$$\frac{d\left(m_1\frac{dR_1}{dt}\right)}{dt} = \frac{\partial}{\partial R_1}\frac{1}{2}LI^2$$

$$m_2\frac{d^2R_2}{dt^2} = \frac{\partial}{\partial R_2}\frac{1}{2}LI^2$$

$$L_1 = \frac{\mu l}{2\pi}\left(ln\frac{a}{R_1} + \frac{1}{N_1}ln\frac{R_1}{N_1R_{w1}}\right)$$

$$L_2 = \frac{\mu l}{2\pi}\left(ln\frac{a}{R_2} + \frac{1}{N_2}ln\frac{R_2}{N_2R_{w2}}\right)$$

$$M = \frac{\mu_0 l}{2\pi}ln\frac{a}{\max(R_1,R_2)}$$

$$\Phi = L_1I_1 + MI_2 = L_2I_2 + MI_1 = LI$$

$$L = \frac{L_1L_2 - M^2}{L_1 + L_2 - 2M}$$

$$V = \frac{d\Phi}{dt}. \tag{2}$$

The indices 1 and 2 are used for the outer and inner arrays, respectively. The wire core array masses and positions are represented by m_i and r_i, respectively. The wire core mass of the outer array m_1, as indicated in the form of its momentum change in (2), is allowed to vary in time, while that of the inner one, m_2, is assumed not to vary. L_i, L, and M are the inductances, total inductance, and mutual inductance, respectively. Φ is the flux seen by the generator, whose time derivative is the load voltage. The return cage radius is denoted by a, and the load length is denoted by l, while N_i and R_i denote the number of wires and wire initial (cold) radii, respectively. The R_i's stay constant throughout the calculation (they do not necessarily have to be the initial radii; the user could use other values as desired). Also, for $N_iR_i \geq 1$, for either or both arrays, the corresponding array inductance becomes that of an infinitesimally thin shell.

It should be noticed that the only way in which the equations reflect inner or outer arrays is by the mutual inductance dependence on array position; therefore, the outer and inner switch roles depending on whether $R_1 > R_2$ or vice versa. As stated before, only the wire core mass of the initially outer array is allowed to vary in a manner that we will discuss next.

Momentum transfer between the wire cores of the arrays when they coincide radially is taken into account by the introduction of a parameter named f_{mom}, whose value, between 0 and 1, is to be selected by the user. For $f_{mom} = 0$, there is no momentum exchange (this is the so-called transparent case), while for $f_{mom} = 1$, the two arrays stick after the collision.

The collision between the two arrays, considered instantaneous, takes place when $R_1(t) = R_2(t)$, with the proviso that this occurs only once, i.e., upon collision the outer array

becomes the inner and vice versa; then, if, at a later time, the originally inner array happens to overtake the originally outer one, the two arrays are made to stick thereafter. Otherwise, the initially outer array gets to the prescribed final radius before the original inner.

The equations describing the momentum exchange are

$$u_i^a = u_i^b - f_{mom}\left(u_i^b - u\right)$$

$$u = \frac{m_1 u_1^b + m_2 u_2^b}{m_1 + m_2} = \frac{m_1 u_1^a + m_2 u_2^a}{m_1 + m_2} = \frac{P_{tot}}{m_1 + m_2}$$

where u denotes velocities and the superscripts (a,b) indicate before and after the instantaneous collision taking place when $R_1(t) = R_2(t)$. By construction, the total momentum P_{tot} is conserved upon this instantaneous collision.

B. Wire Ablation of Outer Array: Rocket Model [30]

The momentum per unit length equation for the outer array precursor plasma is

$$u_{abl}\frac{d\mu}{dt} = F(t), \quad \mu = m/l$$

$$F(t) = -\frac{I^2}{100r(t)} dyn/cm$$

with I in amperes and r in centimeters (all quantities pertaining to the outer array).

During the outer ablation phase, the outer core positions do not change, while the inner code positions are allowed to move according to (2).

Whenever the remaining mass of the core attains in its decrease a prescribed fraction, less than 1, of its initial value, the snowplow phase starts.

C. Snowplow Phase for Outer Array

The snowplow phase momentum equation is $d(\mu u)/dr = F(t)$ with the rate of mass accretion given by (all quantities pertaining to the outer array)

$$\frac{d\mu}{dt} = \frac{d\mu}{dt_o}\frac{dt_0}{dt}$$

where $t_0 = (t - (r(t) - r(t0)))/u_{abl}$.

Thus

$$\frac{d\mu}{dt} = -\frac{d\mu}{dt_0}\frac{u(t) + u_{abl}}{u_{abl}}$$

where $d\mu/dt_0 = F(t_0)/u_{abl}$.

As in the ablation phase, the inner array is advanced using (2) with constant initial mass. No interaction is assumed between the outer array precursor (ablated) plasma and the inner array; only the cores are allowed to exchange momentum as described earlier.

The model allows for the option of leaving behind a fraction f_{behind} of the outer array core mass at the end of the ablation process; the surviving core mass is then multiplied *ad hoc* by $1 - f_{behind}$, with all other equations for the snowplow phase remaining the same as described earlier.

The calculation is stopped when the inner and outer arrays reach prescribed minimum radii.

ACKNOWLEDGMENT

The authors would like to thank the Z operations, the Z diagnostics teams, and the ZBL laser staff at Sandia and A. Finch and J. Worley at Imperial College. The authors would also like to thank C. A. Coverdale (Sandia National Laboratories) for useful comments on the manuscript.

REFERENCES

[1] M. E. Cuneo, D. B. Sinars, E. M. Waisman, D. E. Bliss, W. A. Stygar, R. A. Vesey, R. W. Lemke, I. C. Smith, P. K. Rambo, J. L. Porter, G. A. Chandler, T. J. Nash, M. G. Mazarakis, R. G. Adams, E. P. Yu, K. W. Struve, T. A. Mehlhorn, S. V. Lebedev, J. P. Chittenden, and C. A. Jennings, "Compact single and nested tungsten-wire-array dynamics at 14–19 MA and applications to inertial confinement fusion," *Phys. Plasmas*, vol. 13, no. 5, p. 056318, May 2006.

[2] M. E. Cuneo, R. A. Vesey, G. R. Bennett, D. B. Sinars, W. A. Stygar, E. M. Waisman, J. L. Porter, P. K. Rambo, I. C. Smith, S. V. Lebedev, J. P. Chittenden, D. E. Bliss, T. J. Nash, G. A. Chandler, B. B. Afeyan, E. P. Yu, R. B. Campbell, R. G. Adams, D. L. Hanson, T. A. Mehlhorn, and M. K. Matzen, "Topical review: Progress in symmetric ICF capsule implosions and wire-array z-pinch source physics for double-pinch-driven hohlraums," *Plasma Phys. Control. Fusion*, vol. 48, no. 2, p. R1, Feb. 2006.

[3] J. Lindl, "Development of the indirect-drive approach to inertial confinement fusion and the target physics basis for ignition and gain," *Phys. Plasmas*, vol. 2, no. 11, pp. 3933–4024, Nov. 1995.

[4] S. N. Bland, S. V. Lebedev, J. P. Chittenden, C. Jennings, and M. G. Haines, "Nested wire array Z-pinch experiments operating in the current transfer mode," *Phys. Plasmas*, vol. 10, no. 4, pp. 1100–1112, Apr. 2003.

[5] R. A. Vesey, M. C. Herrmann, R. W. Lemke, M. P. Desjarlais, M. E. Cuneo, W. A. Stygar, G. R. Bennett, R. B. Campbell, P. J. Christenson, T. A. Mehlhorn, J. L. Porter, and S. A. Slutz, "Target design for high fusion yield with the double Z-pinch-driven hohlraum," *Phys. Plasmas*, vol. 14, no. 5, p. 056302, May 2007.

[6] D. D. Ryutov, M. S. Derzon, and M. K. Matzen, "The physics of fast Z pinches," *Rev. Mod. Phys.*, vol. 72, no. 1, pp. 167–223, 2000.

[7] S. V. Lebedev, J. P. Chittenden, F. N. Beg, S. N. Bland, A. Ciardi, D. Ampleford, S. Hughes, M. G. Haines, A. Frank, E. G. Blackman, and T. Gardiner, "Laboratory astrophysics and collimated stellar outflows: The production of radiatively cooled hypersonic plasma jets," *Astrophys. J.*, vol. 564, no. 1, pp. 113–119, Jan. 2002.

[8] S. V. Lebedev, D. Ampleford, A. Ciardi, S. N. Bland, J. P. Chittenden, M. G. Haines, A. Frank, E. G. Blackman, and A. Cunningham, "Jet deflection via crosswinds: Laboratory astrophysical studies," *Astrophys. J.*, vol. 616, no. 2, pp. 988–997, Dec. 2004.

[9] D. J. Ampleford, S. V. Lebedev, A. Ciardi, S. N. Bland, S. C. Bott, J. P. Chittenden, G. Hall, C. A. Jennings, J. Armitage, G. Blyth, S. Christie, and L. Rutland, "Formation of working surfaces in radiatively cooled laboratory jets," *Astrophys. Space Sci.*, vol. 298, no. 1/2, pp. 241–246, Jul. 2005.

[10] D. J. Ampleford, S. V. Lebedev, A. Ciardi, S. N. Bland, S. C. Bott, G. N. Hall, N. Naz, C. A. Jennings, M. Sherlock, J. P. Chittenden, A. Frank, and E. Blackman, "Laboratory modeling of standing shocks and radiatively cooled jets with angular momentum," *Astrophys. Space Sci.*, vol. 307, no. 1–3, pp. 51–56, Jan. 2007.

[11] D. J. Ampleford, A. Ciardi, S. V. Lebedev, S. N. Bland, S. C. Bott, J. P. Chittenden, G. N. Hall, A. Frank, and E. Blackman, "Jet deflection by a quasi-steady-state side wind in the laboratory," *Astrophys. Space Sci.*, vol. 307, no. 1–3, pp. 29–34, Jan. 2007.

[12] D. J. Ampleford, S. V. Lebedev, A. Ciardi, S. N. Bland, S. C. Bott, G. N. Hall, N. Naz, C. A. Jennings, M. Sherlock, J. P. Chittenden, J. B. A. Palmer, A. Frank, and E. Blackman, "Supersonic radiatively cooled rotating flows and jets in the laboratory," *Phys. Rev. Lett.*, vol. 100, no. 3, p. 035001, Jan. 2008.

[13] D. J. Ampleford, S. V. Lebedev, J. P. Chittenden, S. N. Bland, S. C. Bott, G. N. Hall, J. B. A. Palmer, J. Rapley, V. L. Kantsyrev, A. S. Safronova, V. V. Ivanov, D. A. Fedin, P. J. Laca, V. I. Sotnikov, F. Yilmaz, N. Ouart, V. Nalajala, I. Shrestha, S. Pokala, B. Jones, C. Deeney, C. A. Coverdale, and P. D. Lepell, "Implosion dynamics in conical wire array Z-pinches," in *AIP Conf. Proc. 808—Dense Z-Pinches*, 2006, pp. 33–36.

[14] D. J. Ampleford, S. V. Lebedev, S. N. Bland, S. C. Bott, J. P. Chittenden, C. A. Jennings, V. L. Kantsyrev, A. S. Safronova, V. V. Ivanov, D. A. Fedin, P. J. Laca, M. F. Yilmaz, V. Nalajala, I. Shrestha, K. Williamson, G. Osborne, A. Haboub, and A. Ciardi, "Dynamics of conical wire array Z-pinch implosions," *Phys. Plasmas*, vol. 14, no. 10, p. 102704, Oct. 2007.

[15] S. V. Lebedev, R. Aliaga-Rossel, S. N. Bland, J. P. Chittenden, A. E. Dangor, M. G. Haines, and M. Zakaullah, "Two different modes of nested wire array Z-pinch implosions," *Phys. Rev. Lett*, vol. 84, no. 8, pp. 1708–1711, Feb. 2000.

[16] M. E. Cuneo, D. B. Sinars, D. E. Bliss, E. M. Waisman, J. L. Porter, W. A. Stygar, S. V. Lebedev, J. P. Chittenden, G. S. Sarkisov, and B. B. Afeyan, "Direct experimental evidence for current-transfer mode operation of nested tungsten wire arrays at 16-19 MA," *Phys. Rev. Lett.*, vol. 94, no. 22, p. 225 003, Jun. 2005.

[17] E. M. Waisman, "Wire ablation circuit code and evaluation of plasma precursor density width," in *Proc. 5th Int. Workshop Phys. Wire Array Z-Pinches*, 2004, pp. 1–18.

[18] E. M. Waisman, M. E. Cuneo, D. B. Sinars, H. C. Harjes, W. A. Stygar, K. W. Struve, and D. D. Hinshelwood, "Implosion time circuit optimization study of ICF wire array loads for Sandia ZR facility," in *Proc. IEEE Int. Conf. Plasma Sci.*, 2004, p. 360.

[19] E. M. Waisman, M. E. Cuneo, D. B. Sinars, K. W. Struve, C. Deeney, and P. D. LePell, "Array on array circuit studies for ICF radiation pulse tailoring," in *Proc. IEEE Int. Conf. Plasma Sci.*, 2002, p. 106.

[20] R. B. Spielman, "Diamond photoconducting detectors as high power Z-pinch diagnostics (invited)," *Rev. Sci. Instrum.*, vol. 66, no. 1, pp. 867–870, Jan. 1995.

[21] G. A. Chandler, C. Deeney, M. Cuneo, D. L. Fehl, J. S. McGurn, R. B. Spielman, J. A. Torres, J. L. McKenney, J. Mills, and K. W. Struve, "Filtered x-ray diode diagnostics fielded on the Z accelerator for source power measurements," *Rev. Sci. Instrum.*, vol. 70, no. 1, pp. 561–565, Jan. 1999.

[22] R. B. Spielman, C. Deeney, D. L. Fehl, D. L. Hanson, N. R. Keltner, J. S. McGurn, and J. L. McKenney, "Fast resistive bolometry," *Rev. Sci. Instrum*, vol. 70, no. 1, pp. 651–655, Jan. 1999.

[23] R. B. Spielman, C. Deeney, G. A. Chandler, M. R. Douglas, D. L. Fehl, M. K. Matzen, D. H. McDaniel, T. J. Nash, J. L. Porter, T. W. L. Sanford, J. F. Seamen, W. A. Stygar, K. W. Struve, S. P. Breeze, J. S. McGurn, J. A. Torres, D. M. Zagar, T. L. Gilliland, D. O. Jobe, J. L. McKenney, R. C. Mock, M. Vargas, T. Wagoner, and D. L. Peterson, "Tungsten wire-array Z-pinch experiments at 200 TW and 2 MJ," *Phys. Plasmas*, vol. 5, no. 5, pp. 2105–2111, May 1998.

[24] I. H. Mitchell, J. M. Bayley, J. P. Chittenden, J. F. Worley, A. E. Dangor, M. G. Haines, and P. Choi, "A high impedance mega-ampere generator for fiber Z-pinch experiments," *Rev. Sci. Instrum.*, vol. 67, no. 4, pp. 1533–1541, Apr. 1996.

[25] H. Calamy, F. Lassalle, A. Loyen, F. Zucchini, J. P. Chittenden, F. Hamann, P. Maury, A. Georges, J. P. Bedoch, and A. Morell, "Use of microsecond current prepulse for dramatic improvements of wire array Z-pinch implosion," *Phys. Plasmas*, vol. 15, no. 1, p. 012701, Jan. 2008.

[26] S. N. Bland, D. J. Ampleford, S. C. Bott, S. V. Lebedev, J. B. A. Palmer, S. A. Pikuz, and T. A. Shelkovenko, "Extreme ultraviolet imaging of wire array Z-pinch experiments," *Rev. Sci. Instrum.*, vol. 75, no. 10, pp. 3941–3943, Oct. 2004.

[27] S. V. Lebedev, F. N. Beg, S. N. Bland, J. P. Chittenden, A. E. Dangor, and M. G. Haines, "Snowplow-like behavior in the implosion phase of wire array Z pinches," *Phys. Plasmas*, vol. 9, no. 5, pp. 2293–2301, May 2002.

[28] D. B. Sinars, G. R. Bennett, D. F. Wenger, M. E. Cuneo, D. L. Hanson, J. L. Porter, R. G. Adams, P. K. Rambo, D. C. Rovang, and I. C. Smith, "Monochromatic x-ray imaging experiments on the Sandia National Laboratories Z facility (invited)," *Rev. Sci. Instrum.*, vol. 75, no. 10, pp. 3672–3677, Oct. 2004.

[29] A. L. Velikovich, I. V. Sokolov, and A. A. Esaulov, "Perfectly conducting incompressible fluid model of a wire array implosion," *Phys. Plasmas*, vol. 9, no. 4, pp. 1366–1380, Apr. 2002.

[30] S. V. Lebedev, F. N. Beg, S. N. Bland, J. P. Chittenden, A. E. Dangor, M. G. Haines, K. H. Kwek, S. A. Pikuz, and T. A. Shelkovenko, "Effect of discrete wires on the implosion dynamics of wire array Z-pinches," *Phys. Plasmas*, vol. 8, no. 8, pp. 3734–3747, Aug. 2001.

D. J. Ampleford received the M.Sci. and Ph.D. degrees from Imperial College London, London, U.K., in 2001 and 2005, respectively. His Ph.D. thesis work used the MAGPIE generator for laboratory astrophysics modeling of protostellar jets using conical wire Z-pinches.

In 2005, he joined Sandia National Laboratories, Albuquerque, NM. He is currently a member of the Technical Staff in the Radiation and Fusion Experiments group at Sandia. His research includes performing experiments with large-diameter wire-array Z-pinches to produce K-shell emission on the Z generator, performing experiments with novel wire-array configurations on the Saturn and MAGPIE generators, and a continued interest in high-energy-density laboratory astrophysics. He has published 60 peer-reviewed papers on topics including wire-array Z-pinches and laboratory astrophysics.

S. N. Bland, photograph and biography not available at the time of publication.

M. E. Cuneo, photograph and biography not available at the time of publication.

S. V. Lebedev, photograph and biography not available at the time of publication.

D. B. Sinars (M'04) received the B.S. degree in engineering physics from the University of Oklahoma, Norman, in 1996 and the Ph.D. degree in applied physics from Cornell University, Ithaca, NY, in 2001. His dissertation was on time-resolved measurements of plasma conditions in X-pinch plasmas using X-ray spectroscopy.

From 2001 to present, he has worked at Sandia National Laboratories, Albuquerque, NM, in the areas of inertial confinement fusion, Z-pinch physics, and high-energy-density physics. He has conducted over 160 experiments on the "Z" pulsed-power facility in these areas and led the development of numerous X-ray and spectroscopy diagnostics for the facility. The most notable example is the monochromatic X-ray backlighting diagnostics, which are currently the primary radiographic technique for the facility. He has published over 85 papers in peer-reviewed journals.

Dr. Sinars received the 2007 IEEE Nuclear Plasma Sciences Society Early Achievement Award, and he recently received both the 2011 Department of Energy Early Career Award and the 2011 Presidential Early Career Award for Scientists and Engineers for his work.

C. A. Jennings received the M.Sci. degree in physics and the Ph.D. degree in computational modeling of wire-array Z-pinches from Imperial College London, London, U.K., in 2005.

Since 2006, he has been with the ICF Target Design Group, Sandia National Laboratories, Albuquerque, NM, where he continues to work on the computational modeling of wire-array Z-pinches.

E. M. Waisman received the Ph.D. degree in physics from Yeshiva University in 1970.

He has been a Consultant for the Pulsed Power Center of Sandia National Laboratories, Albuquerque, NM, since 2001. As part of his consultancy at Sandia, he developed circuit representations of wire arrays and gas puff loads for ICF and K-shell applications. He has designed data analysis techniques to extract load behavior from electrical data, studied radiatively driven vacuum-gap closure, collaborated in the development of the 3-D RMHD code ALEGRA, and researched X-ray power scaling for wire-array Z-pinch-driven ICF technology. He has also contributed to the design of low inductance vacuum lines and vacuum voltage diagnostics. He was the President of the S-Cubed Division of Maxwell, from 1994 to 1996, with total personnel of over 200 and science and technology programs of over $25 million/year. During more than 20 years at Maxwell, he also served as the Manager of the Plasma Physics Group (1989–1992), the Vice President of the X-ray Pulsed Power Simulators Sector of the Balboa Division (1992–1994), and the Head of the Theory Group of Maxwell Physics International (1998–2001). He was the Vice President of Alameda Applied Sciences, Inc., from 2001 to 2003. He has 35 years of experience working in the physics and technology of pulsed power encompassing the following: power flow in vacuum for pulsed-power technology, plasma opening switches, plasma radiation sources, both wire arrays and gas puffs, electron and ion beams as loads of pulsed-power generators, as well as in the fields of electromagnetic pulses and railgun physics. He has also worked in the area of statistical mechanics.

R. A. Vesey, photograph and biography not available at the time of publication.

G. N. Hall, photograph and biography not available at the time of publication.

F. Suzuki-Vidal received the B.Sc. degree in physics from Pontificia Universidad Católica de Chile, Santiago, Chile, in 2004, with the Optics and Plasma Physics group. He received the Ph.D. degree in physics from Imperial College London, London, U.K., in 2009, with a thesis on the Experimental Study of Radiatively Cooled Magnetically Driven Plasma Jets with the Plasma Physics group.

He is currently a Research Associate with Imperial College London, working on experiments related to high-energy-density laboratory plasma astrophysics of supersonic flows and radiative shocks.

J. P. Chittenden (M'07) received the B.Sc. degree in physics from the University College London, London, U.K., in 1987 and the Ph.D. degree in plasma physics from Imperial College London, London, in 1990.

He was appointed to the faculty of Imperial College in 2003 and became a Professor of Plasma Physics in 2011. His research interests are principally centered on magnetized high energy density plasmas. He has published more than 100 journal articles on Z-pinches, inertial confinement, fusion, X-pinch plasmas, X-ray lasers, laboratory astrophysics, multidimensional magnetohydrodynamic modeling, and pulsed-power engineering.

Prof. Chittenden is a Fellow of the American Physical Society and currently serves on the IEEE Plasma Science and Applications Executive Committee.

S. C. Bott (M'07) received the M.Phys. (Chem.Phys.) and Ph.D. degrees from Sheffield University, Sheffield, U.K., in 1999 and 2003, respectively. His Ph.D. thesis work investigated low-density deuterium discharges for UV lighting applications.

In 2003, he joined the Plasma Physics Group at Imperial College, London, U.K., where he extensively investigated the ablation of wire-array Z-pinches. In 2006, he joined the University of California San Diego, La Jolla, as an Assistant Project Scientist in the High Energy Density Physics group. He took up his current position in 2010. He is an Assistant Research Scientist at the University of California San Diego's Center for Energy Research and leads the Pulsed Power Plasmas Group. His research interests include the basic physics of plasmas generated by pulse power machines and their application in broader plasma science, laboratory astrophysics, and inertial confinement fusion. He has published over 50 journal articles on pulsed-power plasmas.

Dr. Bott served on the Program Committee for the 7th and the 8th International Conference on Dense Z-Pinches, in various roles for the ICOPS conference series, and as a Guest Editor for the 4th and 5th Special Issues on Z-Pinch Plasmas published in the IEEE TRANSACTIONS ON PLASMA SCIENCE.